



Probing the origin of highly-efficient third-harmonic generation in plasmonic nanogaps

QIXIN SHEN,¹ THANG B. HOANG,¹ GUOCE YANG,² VIRGINIA D. WHEELER,³
AND MAIKEN H. MIKKELSEN^{1,2,4}

¹Department of Physics, Duke University, Durham, NC 27708, USA

²Department of Electrical and Computer Engineering, Duke University, Durham, NC 27708, USA

³United States Naval Research Laboratory, Washington, DC 20375, USA

⁴m.mikkelsen@duke.edu

Abstract: Plasmonic structures can precisely localize electromagnetic energy to deep subwavelength regions resulting in significant field enhancement useful for efficient on-chip nonlinear generation. However, the origin of large nonlinear enhancements observed in plasmonic nanogap structures consisting of both dielectrics and metals is not fully understood. For the first time, here we probe the third harmonic generation (THG) from a variety of dielectric materials embedded in a nanogap plasmonic cavity. From comprehensive spectral analysis of the THG signal, we conclude that the nonlinear response results primarily from the dielectric spacer layer itself as opposed to the surrounding metal. We achieved a maximum enhancement factor of more than six orders of magnitude compared to a bare gold film, which represents a nonlinear conversion efficiency of $8.78 \times 10^{-4}\%$. We expect this new insight into the nonlinear response in ultrathin gaps between metals to be promising for on-chip nonlinear devices such as ultrafast optical switching and entangled photon sources.

© 2018 Optical Society of America under the terms of the OSA Open Access Publishing Agreement

OCIS codes: (250.5403) Plasmonics; (160.4330) Nonlinear optical materials; (190.2620) Harmonic generation and mixing; (190.4360) Nonlinear optics, devices; (190.7110) Ultrafast nonlinear optics.

References and links

1. G. Grinblat, Y. Li, M. P. Nielsen, R. F. Oulton, and S. A. Maier, "Enhanced third harmonic generation in single germanium nanodisks excited at the anapole mode," *Nano Lett.* **16**(7), 4635–4640 (2016).
2. M. R. Shcherbakov, D. N. Neshev, B. Hopkins, A. S. Shorokhov, I. Staude, E. V. Melik-Gaykazyan, M. Decker, A. A. Ezhov, A. E. Miroshnichenko, I. Brener, A. A. Fedyanin, and Y. S. Kivshar, "Enhanced third-harmonic generation in silicon nanoparticles driven by magnetic response," *Nano Lett.* **14**(11), 6488–6492 (2014).
3. J. B. Lassiter, X. Chen, X. Liu, C. Ciraci, T. B. Hoang, S. Larouche, S. H. Oh, M. H. Mikkelsen, and D. R. Smith, "Third-harmonic generation enhancement by film-coupled plasmonic stripe resonators," *ACS Photonics* **1**(11), 1212–1217 (2014).
4. H. Aouani, M. Rahmani, M. Navarro-Cía, and S. A. Maier, "Third-harmonic-upconversion enhancement from a single semiconductor nanoparticle coupled to a plasmonic antenna," *Nat. Nanotechnol.* **9**(4), 290–294 (2014).
5. B. Metzger, M. Hentschel, T. Schumacher, M. Lippitz, X. Ye, C. B. Murray, B. Knabe, K. Buse, and H. Giessen, "Doubling the efficiency of third harmonic generation by positioning ITO nanocrystals into the hot-spot of plasmonic gap-antennas," *Nano Lett.* **14**(5), 2867–2872 (2014).
6. A. Lesuffleur, L. K. S. Kumar, and R. Gordon, "Enhanced second harmonic generation from nanoscale double-hole arrays in a gold film," *Appl. Phys. Lett.* **88**(26), 261104 (2006).
7. P. Genevet, J. P. Tetienne, E. Gatzogiannis, R. Blanchard, M. A. Kats, M. O. Scully, and F. Capasso, "Large enhancement of nonlinear optical phenomena by plasmonic nanocavity gratings," *Nano Lett.* **10**(12), 4880–4883 (2010).
8. G. M. Akselrod, C. Argyropoulos, T. B. Hoang, C. Ciraci, C. Fang, J. Huang, D. R. Smith, and M. H. Mikkelsen, "Probing the mechanisms of large Purcell enhancement in plasmonic nanoantennas," *Nat. Photonics* **8**(11), 835–840 (2014).
9. J. B. Lassiter, F. McGuire, J. J. Mock, C. Ciraci, R. T. Hill, B. J. Wiley, A. Chilkoti, and D. R. Smith, "Plasmonic waveguide modes of film-coupled metallic nanocubes," *Nano Lett.* **13**(12), 5866–5872 (2013).
10. G. M. Akselrod, J. Huang, T. B. Hoang, P. T. Bowen, L. Su, D. R. Smith, and M. H. Mikkelsen, "Large-area Metasurface perfect absorbers from visible to near-Infrared," *Adv. Mater.* **27**(48), 8028–8034 (2015).
11. M. Kauranen and A. V. Zayats, "Nonlinear plasmonics," *Nat. Photonics* **6**(11), 737–748 (2012).
12. Y. Zhang, N. K. Grady, C. Ayala-Orozco, and N. J. Halas, "Three-dimensional nanostructures as highly efficient generators of second harmonic light," *Nano Lett.* **11**(12), 5519–5523 (2011).
13. A. Nahata, R. A. Linke, T. Ishi, and K. Ohashi, "Enhanced nonlinear optical conversion from a periodically

- nanostuctured metal film,” *Opt. Lett.* **28**(6), 423–425 (2003).
14. A. Bouhelier, M. Beversluis, A. Hartschuh, and L. Novotny, “Near-field second-harmonic generation induced by local field enhancement,” *Phys. Rev. Lett.* **90**(1), 013903 (2003).
 15. Y. Pu, R. Grange, C. L. Hsieh, and D. Psaltis, “Nonlinear optical properties of core-shell nanocavities for enhanced second-harmonic generation,” *Phys. Rev. Lett.* **104**(20), 207402 (2010).
 16. H. Aouani, M. Navarro-Cia, M. Rahmani, and S. A. Maier, “Unveiling the origin of third harmonic generation in hybrid ITO-plasmonic crystals,” *Adv. Opt. Mater.* **3**(8), 1059–1065 (2015).
 17. T. Utikal, T. Zentgraf, T. Paul, C. Rockstuhl, F. Lederer, M. Lippitz, and H. Giessen, “Towards the origin of the nonlinear response in hybrid plasmonic systems,” *Phys. Rev. Lett.* **106**(13), 133901 (2011).
 18. Y. Zhang, F. Wen, Y.-R. Zhen, P. Nordlander, and N. J. Halas, “Coherent Fano resonances in a plasmonic nanocluster enhance optical four-wave mixing,” *Proc. Natl. Acad. Sci. U.S.A.* **110**(23), 9215–9219 (2013).
 19. J. Renger, R. Quidant, N. van Hulst, and L. Novotny, “Surface-enhanced nonlinear four-wave mixing,” *Phys. Rev. Lett.* **104**(4), 046803 (2010).
 20. D. Débarre, W. Supatto, A.-M. Pena, A. Fabre, T. Tordjmann, L. Combettes, M.-C. Schanne-Klein, and E. Beaurepaire, “Imaging lipid bodies in cells and tissues using third-harmonic generation microscopy,” *Nat. Methods* **3**(1), 47–53 (2006).
 21. C. Min, P. Wang, C. Chen, Y. Deng, Y. Lu, H. Ming, T. Ning, Y. Zhou, and G. Yang, “All-optical switching in subwavelength metallic grating structure containing nonlinear optical materials,” *Opt. Lett.* **33**(8), 869–871 (2008).
 22. J. R. DeVore, “Refractive Indices of Rutile and Sphalerite,” *J. Opt. Soc. Am.* **41**(6), 416 (1951).
 23. I. H. Malitson and M. J. Dodge, “Refractive index and birefringence of synthetic sapphire,” *J. Opt. Soc. Am.* **62**(11), 1405 (1972).
 24. R. J. Moerland and J. P. Hoogenboom, “Subnanometer-accuracy optical distance ruler based on fluorescence quenching by transparent conductors,” *Optica* **3**(2), 112 (2016).
 25. D. L. Wood, K. Nassau, T. Y. Kometani, and D. L. Nash, “Optical properties of cubic hafnia stabilized with yttria,” *Appl. Opt.* **29**(4), 604–607 (1990).
 26. R. W. Boyd, *Nonlinear Optics* (Academic, 2008).

1. Introduction

The efficiency of nonlinear generation can be enhanced by taking advantage of nanostructures that mold the local electromagnetic fields, such as all-dielectric nanodisks [1,2], metallic nanoantennas [3–5], and patterned gold film [6,7]. Plasmonic nanostructures are especially promising as surface plasmon polaritons can confine light to volumes much smaller than the diffraction limit of light [8–10], resulting in greatly enhanced local electromagnetic fields which also results in relaxed phase matching conditions [11]. A variety of nonlinear processes have been studied including second harmonic generation (SHG) [6,7,12–15], third harmonic generation (THG) [1–5,16,17], and four wave mixing (FWM) [7,18,19]. Among these nonlinear processes, THG has attracted great interest since symmetry breaking is not required and it plays a key role for nonlinear imaging [20] and optical switching [21]. Plasmonic enhancement of THG have been studied in bowtie [4,5], nanowire [17], and gap-plasmon structures [3]; however, open questions still remain as to the main source of the nonlinear response in such hybrid systems consisting of both metals and dielectrics.

Here, we utilize spectral analysis and a variety of dielectric materials to investigate the main source of the THG response in a hybrid plasmonic structure, namely the film-coupled gold nanostripe resonator, as well as demonstrate a large nonlinear enhancement and high conversion efficiency. A comprehensive investigation of the THG response for different nanostripe widths, excitation wavelengths and gap thicknesses indicate that the THG response mainly originates from the dielectric layer itself.

2. Results

A schematic of the sample structure is shown in Fig. 1(a), consisting of a thin dielectric layer sandwiched between a 75 nm gold film and gold nanostripes fabricated by electron-beam lithography (EBL). Four different dielectric materials with thicknesses between 1 and 5 nm are studied here: Al_2O_3 , HfO_2 , and TiO_2 deposited by atomic layer deposition (ALD) and ITO deposited by sputtering. The chosen thickness for each material was the thinnest that could reliably be fabricated while maintaining a continuous and uniform layer on top of the gold film. The stripe widths were characterized by scanning electron microscope (SEM) and

ellipsometry was used to measure the thickness of the dielectric layers. The period between the stripes was kept constant for all measurements at 250 nm while the stripe widths were varied to achieve a variety of plasmonic resonances.

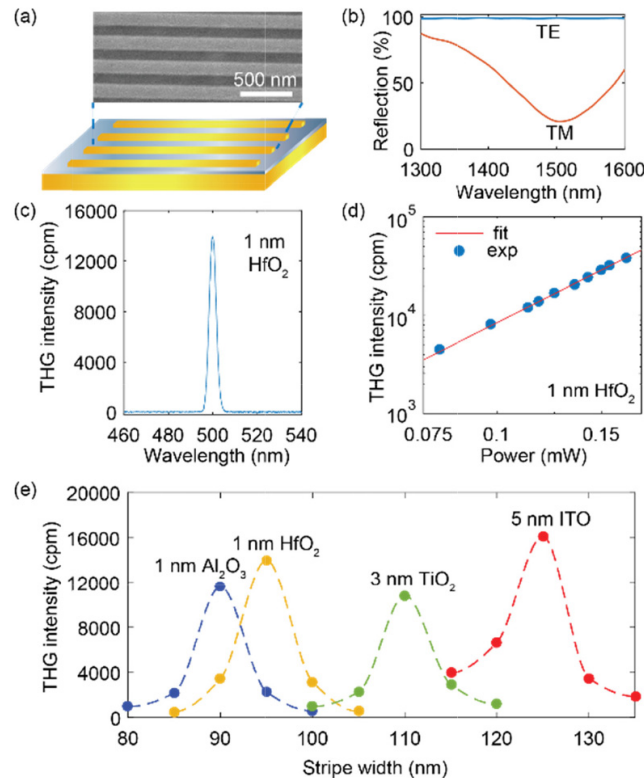


Fig. 1. (a) Schematic and SEM image of the sample structure consisting of a thin dielectric layer sandwiched between a gold film and stripes. (b) Measured reflection spectra from an array of stripes for an incident polarization perpendicular to the stripes (transverse magnetic (TM)) and parallel to the stripes (transverse electric (TE)). (c) Representative spectrum of THG from 95 nm stripes for TM polarization. (d) THG intensity from stripes as a function of excitation power confirming a third order power dependence. (e) Dependence of THG intensity on the width of the gold stripes for four different dielectric spacers as indicated in the figure. Dots represent experimental data and dashed lines are guides to the eye.

The structure acts as a plasmonic nanocavity which localizes and strongly enhances the optical field [8–10] when excited with light polarized perpendicular to the stripes (Fig. 1(b)), whereas no absorption is observed for a polarization along the stripes as localized plasmon resonances are not supported. Therefore, all samples were excited with light polarized perpendicular to the stripes and an excitation wavelength of 1500 nm was used for all experiments (except wavelength dependence measurements). In order to match the plasmon resonance of the structure with the fixed excitation wavelength, white light absorption measurements were performed on each sample to determine the specific stripe width resulting in a plasmon resonance centered at 1500 nm. A characteristic THG signal is observed at 500 nm (Fig. 1(c)), using a home-built microscope in a reflective configuration, for a sample with a 1 nm HfO₂ layer. To verify that the peak is indeed from the THG process, we performed excitation power dependence measurements on the stripes and the nearby dielectric-metal film (without stripes) as a control for each sample, as well as on a bare gold film (with no dielectric material). Figure 1(d) shows the THG intensity as a function of incident laser power from the film-coupled nanostructures with a 1 nm layer of HfO₂. A polynomial function fit

reveals a slope of 3.03, very close to three as is expected from the third order nonlinear process. Similarly, we have also confirmed the THG response from the other samples with different dielectric materials as well as the bare gold film by verifying the third power law. This allows for the intensities measured at different powers to be interpolated enabling direct comparison between different samples.

As a first step to elucidate the main source of the THG enhancement in this plasmonic structure, we explore the fundamental resonance for various widths of the stripes on samples with four different dielectric materials (1 nm Al_2O_3 , 1 nm HfO_2 , 5 nm ITO and 3 nm TiO_2). For each sample, the THG signal was collected from five different arrays of stripes with an incident laser wavelength of 1500 nm. Figure 1(e) reveals the stripe width for each sample that result in the maximum THG response, which is consistent with the specific stripe width that corresponds to an absorption peak at 1500 nm. It is also observed, that the THG response decrease rapidly for stripes with widths corresponding to resonances away from the excitation wavelength. This is expected as nanostripes with a plasmon resonance overlapping with the excitation wavelength at 1500 nm has the maximum localized field intensity and thus the maximum nonlinear response.

To further probe the origin of the nonlinear response, measurements of excitation wavelength dependence were performed. In these experiments, the stripe width of each sample was fixed to ensure a resonance at 1500 nm, and the excitation wavelength was tuned from 1470 nm to 1530 nm. Figures 2(a)-2(d) show the dependence of the THG response on the excitation wavelength for the four samples mentioned above. It is observed that the nonlinear response decrease rapidly when the excitation wavelength is detuned from the 1500 nm resonance. Furthermore, control measurements from areas without stripes show a nearly constant THG signal independent of the excitation wavelength. As high excitation power (10 mW), which was used for the control measurements could lead to damage of the stripes, the intensities shown in Fig. 2 for the stripes were measured at lower excitation powers (0.125–0.25 mW) and interpolated to the power used for the control sample using the third power law verified above (Fig. 1(d)). From Lorentzian fits to the experimental data in Fig. 2, the full width at half maximum (FWHM) was extracted from the different samples. The smallest thickness of 1 nm of HfO_2 has the narrowest FWHM of 25 nm and a relatively large refractive index of 2.07, while the thicker 5 nm ITO has the largest FWHM of 50 nm and a relatively small refractive index of less than 1.6. Generally, it is observed that the FWHM is narrower for thinner dielectric layers and for dielectrics with larger refractive index (as obtained from literature [22–25]) at 1500 nm. The electric field distribution is simulated in this hybrid structure using the experimental dimensions for the sample with a 3 nm TiO_2 dielectric layer (Figs. 2(e)-2(f)). The confined electric field within the dielectric layer in the gap region decreases once the plasmonic structure is even slightly off-resonant with the excitation wavelength from 1500 nm to 1470 nm. The rapid decay of THG intensity from stripes that are off-resonant can be explained by the rapid decay of this localized field intensity. This is also supported by the observation that the THG signal from areas without stripes does not exhibit any significant dependence on the excitation wavelength. Thus, the THG response is strongly related to the enhanced field intensity confined within the dielectric layer pointing towards the dielectric layer contributing significantly to the observed THG.

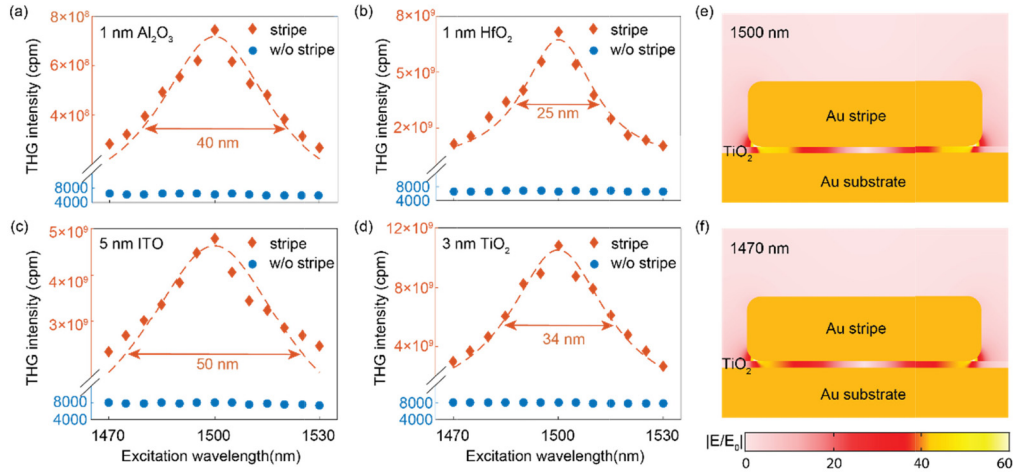


Fig. 2. (a-d) Excitation wavelength dependence of THG intensity for four different dielectric materials embedded in the nanostructure. The excitation wavelength is tuned around 1500 nm at 5 nm intervals. Red diamonds are experimental data from stripes that were interpolated to the same excitation power as used for areas without stripes, while blue dots are experimental data from areas without stripes. The dashed red curve is a Lorentzian function fit. (e-f) Simulated electric field distribution for excitation wavelengths of 1500 nm (on resonance) and 1470 nm (slightly off resonance).

Next, to quantify the THG enhancement in these structures, we selected a bare gold film as a reference since the nonlinear response from the very thin dielectric layers alone without the underlying gold film is inherently too weak to observe. The THG enhancement is thus defined here as the THG signal from a given sample divided by the THG signal from a gold reference sample using the same excitation wavelength and power. We observe that for the two Al₂O₃ samples, the THG intensity increases by more than two orders of magnitude as the gap thickness is decreased from 3 to 1 nm as shown in Table 1. Additionally, almost an order of magnitude larger THG enhancement is observed for 1 nm of HfO₂ embedded in the nanostructures as compared with 1 nm of Al₂O₃. This large difference between the THG enhancements of the two samples is unlikely originating from the gold films alone because the nonlinear response from the gold areas is similar, given that the electric field intensity within the gold is similar for these two samples. The difference is also unlikely due to any small variation in their cavity volumes, resulting from stripe width variations. Thus, the large difference between the THG enhancements for the two samples must be related to the different dielectric materials in the gap. This observation indicates that, at least for the HfO₂ sample, that the main THG source is the dielectric itself. Further supporting this interpretation is the observation of more than three orders of magnitude larger THG enhancement for the 3 nm TiO₂ sample as compared with the 3 nm Al₂O₃ sample. TiO₂ has a $\chi^{(3)}$ value of 2.1×10^{-20} (m²/V²) which is around two orders of magnitude larger than that of Al₂O₃ (3.1×10^{-22} (m²/V²)) [26], therefore giving rise to a larger THG signal. We also notice that the 5 nm ITO sample has a relatively large enhancement because of its very large $\chi^{(3)}$ value (2.16×10^{-18} (m²/V²)), even though it has a thicker dielectric gap compared with the other samples. Therefore, larger $\chi^{(3)}$ values and thinner gaps are important factors to achieve higher THG enhancement in this hybrid plasmonic structure. Even though the $\chi^{(3)}$ value of HfO₂ has not yet been reported in literature, the observed THG enhancement from our experiments (1 nm HfO₂ vs. 1 nm Al₂O₃) is suggesting that the $\chi^{(3)}$ value of HfO₂ is greater than that of Al₂O₃.

Table 1. THG enhancement factor; efficiency and effective $\chi^{(3)}$ values of film-coupled plasmonic stripe resonators with five different dielectric materials in the gap along with a gold reference sample.

	Gold	3 nm Al ₂ O ₃	1 nm Al ₂ O ₃	1 nm HfO ₂	5 nm ITO	3 nm TiO ₂
THG enhancement	1	10 ^{3.00}	10 ^{5.05}	10 ^{6.03}	10 ^{5.86}	10 ^{6.21}
THG efficiency (%)	2.05 × 10 ⁻⁹	5.06 × 10 ⁻⁷	5.64 × 10 ⁻⁵	5.70 × 10 ⁻⁴	3.58 × 10 ⁻⁴	8.78 × 10 ⁻⁴
Effective $\chi^{(3)}$ (m ² /V ²)	7.6 × 10 ⁻¹⁹	7.6 × 10 ⁻¹⁶	8.5 × 10 ⁻¹⁴	8.2 × 10 ⁻¹³	5.5 × 10 ⁻¹³	1.2 × 10 ⁻¹²

In addition to the large enhancement, the coupled stripe-film system also exhibits a high conversion efficiency from incident excitation energy to THG intensity. The efficiency is defined as the power of the THG response generated from the sample divided by the power of the incident laser. The incident excitation power is measured by a power meter, while the power of the THG response is derived from the CCD counts and is normalized by a calibrated light source (Labsphere). As shown in Table 1, the gold reference sample has a low THG efficiency of $2.05 \times 10^{-9}\%$, while the dielectric samples with stripes can achieve relatively high efficiencies as compared to gold. The highest efficiency observed here was $8.78 \times 10^{-4}\%$ from 3 nm of TiO₂ embedded in the plasmonic film-coupled nanostructures. Different definitions for the THG efficiency used in literature complicates a direct comparison of their absolute values [4]. However, we show that a high efficiency compared with gold can be achieved with the same structure on different materials despite relatively low $\chi^{(3)}$ values of some of the materials. In the experiments here, the excitation power was limited to 5 mW in order to prevent damage of the sample due to the corresponding large localized field intensity. Another figure of merit to enable comparisons to other studies, is an effective $\chi^{(3)}$ value [4] from the sample, which is defined as the product of the $\chi^{(3)}$ value of gold and the corresponding enhancement factor as the same excitation conditions are used. The highest estimated effective $\chi^{(3)}$ value from the dielectric material embedded in the nanostructure is from the 3 nm TiO₂ sample with a value of $1.2 \times 10^{-12}(\text{m}^2/\text{V}^2)$. The effective $\chi^{(3)}$ values from the other dielectric samples are listed in Table 1.

While most previous research focused on the intensity of the THG response, few investigated the shape of the spectrum itself [3–5]. Two dimensional finite difference time domain method (Lumerical FDTD Solutions) was used to calculate the THG spectrum. In the simulation model, periodic boundary conditions were used and the structure was illuminated by a normal incident plane wave pulse source with pulse length of 150 fs and central wavelength of 1500 nm, which were consistent with the experimental conditions. A frequency domain power monitor was used to record the output power through the monitor plane in simulations. In experiment, the FWHM of the 5 nm ITO embedded plasmonic structure is found to be only 3.3 nm whereas it is 4.2 nm from the substrate as shown in Fig. 3(a). This is consistent with the simulation result, where the FWHMs are 3.15 nm and 4.20 nm from the embedded plasmonic structure and substrate, respectively. As seen in Fig. 3(c), the other dielectric materials follow a similar trend, displaying a narrower spectrum from stripes compared with the substrate. An explanation for this narrowing effect is given by considering the contributions from different nonlinear sources in this hybrid structure. When both nonlinearities are considered simultaneously, as is the case in the experimental data, the spectrum is the same as the simulated stripe case shown in Fig. 3(b). However, the simulated spectra behave differently when the nonlinearity of the dielectric material or gold is considered individually. As shown in Fig. 3(d), the nonlinearity of the dielectric material is critical to the narrowing effect of the THG spectrum, while the nonlinearity of the gold alone cannot produce the narrower spectrum which was observed in the experiments. The clear and statistically significant difference between the FWHM of the spectra from the stripes and the substrate is a strong indication that the THG in these structures mainly arise from the dielectric material in the gap.

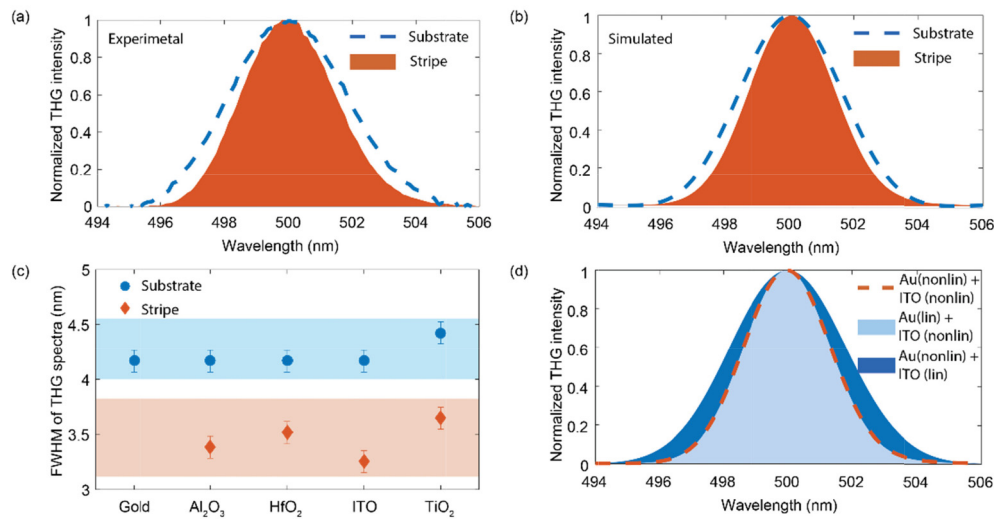


Fig. 3. (a-b) Normalized THG spectra from 5 nm of ITO embedded in the nanostructure compared to the substrate area without stripes (consisting of gold film and dielectric layer). Experimental data is shown in (a) and corresponding simulations in (b). (c) FWHM of THG spectra from four different dielectric samples and the gold reference sample measured using the same excitation conditions. Error bars are obtained based on measurements on five different areas on each sample. (d) Simulated THG spectra by considering the individual contributions from different nonlinear sources in this hybrid structure.

3. Conclusion

In conclusion, greater than six orders of magnitude enhancement in the THG signal was observed from plasmonic film-coupled stripe resonators compared with a bare gold film. To elucidate the origin of the THG signal, a comprehensive study was performed of the film-coupled nanostructure resonators in terms of stripe width, excitation wavelength and dielectric spacer material. Both these experiments and corresponding simulations indicate that the THG response mainly arises from the dielectric layer itself. Despite using an ultrathin layer of dielectric (1-5 nm), high nonlinear conversion efficiency was extracted, which is promising for future on-chip nonlinear devices. Furthermore, as the THG is a process without saturation where the intensity grows cubically as a function of the incident power, the efficiency can be even higher if the damage threshold of the sample can be increased, given more robust metals and dielectric layers. The hybrid plasmonic structure and the large THG enhancement offer a pathway to explore other nonlinear optical processes at the nanoscale, which are promising for future on-chip nonlinear devices such as ultrafast optical switching and entangled photon sources.

Appendix 1. Fabrication

All of the samples used in this work were fabricated by a three-step fabrication process. First, a 75 nm gold film was deposited onto a silicon substrate by electron-beam evaporation with 2 Å/s deposition rate. Second, an ultrathin dielectric layer was deposited on top of the gold film by ALD or sputtering depending on the material. Al₂O₃ and HfO₂ were deposited by ALD by VaporPulse Technologies, Inc. TiO₂ was deposited by ALD in an Ultratech Fiji G2 reactor at 250°C with tetrakis (dimethylamino) titanium (IV) and O₂ plasma (40 sccm) precursors at ~ 12 mTorr, which results in a linear growth rate of 0.55 Å/cycle. ITO was deposited by sputtering with 50W DC power and no substrate heating (Kurt Lesker PVD 75). The last step is EBL fabrication of 30 nm gold stripes on top of the dielectric layer. The gold reference sample used in this work was also prepared under the same conditions, but without the dielectric layer and gold stripes.

Appendix 2. Optical setup

The samples were excited by an optical parametric oscillator pumped by a Ti: sapphire laser (Coherent Chameleon, ~150 fs pulse duration, 80 MHz repetition rate) which were passed through a half-wave plate and focused onto the sample plane via a microscope objective (Mitutoyo M Plan Apo NIR, 50×). The same objective was used to collect the light in a reflection geometry, and the light was then passed through a dichroic mirror along with a short-pass filter (600 nm) before being detected by a CCD-coupled spectrometer (Acton sp2500i).

Appendix 3. Simulation

The range of wavelength in the monitor was set from 400 nm to 700 nm and 6001 frequency points were sampled on the monitor. The simulation bandwidth for mesh generation was overridden by 400 nm to 1600 nm which is suitable for both pump wavelength and THG wavelength.

Funding

Cottrell Scholar award from the Research Corporation for Science Advancement and the Air Force Office of Scientific Research Young Investigator Research Program (AFOSR, Grant No. FA9550-15-1-0301).